AIP | Applied Physics Letters

Anomalous high photoconductivity in short channel indium-zinc-oxide photo-transistors

Hyun-Sik Choi and Sanghun Jeon

Citation: Applied Physics Letters **106**, 013503 (2015); doi: 10.1063/1.4905310
View online: http://dx.doi.org/10.1063/1.4905310
View Table of Contents: http://scitation.aip.org/content/aip/journal/apl/106/1?ver=pdfcov
Published by the AIP Publishing

Articles you may be interested in

Effect of top gate bias on photocurrent and negative bias illumination stress instability in dual gate amorphous indium-gallium-zinc oxide thin-film transistor
Appl. Phys. Lett. **107**, 233509 (2015); 10.1063/1.4937441

Proton induced multilevel storage capability in self-assembled indium-zinc-oxide thin-film transistors
Appl. Phys. Lett. **103**, 113503 (2013); 10.1063/1.4821067

High responsivity of amorphous indium gallium zinc oxide phototransistor with Ta2O5 gate dielectric
Appl. Phys. Lett. **101**, 261112 (2012); 10.1063/1.4773307

Transparent thin-film transistors with zinc indium oxide channel layer
J. Appl. Phys. **97**, 064505 (2005); 10.1063/1.1862767

High-photosensitivity p -channel organic phototransistors based on a biphenyl end-capped fused bithiophene oligomer
Appl. Phys. Lett. **86**, 043501 (2005); 10.1063/1.1856144

This article is copyrighted as indicated in the article. Reuse of AIP content is subject to the terms at: http://scitation.aip.org/termsconditions. Downloaded to IP: 35.8.11.3 On: Tue, 26 Jan 2016 18:52:14

Anomalous high photoconductivity in short channel indium-zinc-oxide photo-transistors

Hyun-Sik Choi[1] and Sanghun Jeon[2,a)]
[1]Semiconductor Device Laboratory, Samsung Advanced Institute of Technology (SAIT), Samsung Electronics Corporation, Gyeonggi 449-712, South Korea
[2]Department of Applied Physics and Department of Display and Semiconductor Physics, Korea University, 2511 Sejongro, Sejong, 339-700, South Korea

(Received 19 November 2014; accepted 18 December 2014; published online 5 January 2015)

Upon light exposure, an indium-zinc-oxide (IZO) thin-film transistor (TFT) presents higher photoconductivity by several orders of magnitude at the negative gate bias region. Among various device geometrical factors, scaling down the channel length of the photo-transistor results in an anomalous increase in photoconductivity. To probe the origin of this high photoconductivity in short-channel device, we measured transient current, current–voltage, and capacitance–voltage characteristics of IZO–TFTs with various channel lengths and widths before and after illumination. Under the illumination, the equilibrium potential region which lies far from front interface exists only in short-channel devices, forming the un-depleted conducting back channel. This region plays an important role in carrier transport under the illumination, leading to high photoconductivity in short-channel devices. Photon exposure coupled with gate-modulated band bending for short-channel devices leads to the accumulation of V_o^{++} at the front channel and screening negative gate bias, thereby generating high current flow in the un-depleted back-channel region. © *2015 AIP Publishing LLC*.
[http://dx.doi.org/10.1063/1.4905310]

Indium-zinc-oxide (IZO) semiconductor thin-film transistors (TFTs) have attracted tremendous attention as a switch element in next-generation display devices owing to their electrical and optical properties as well as ease of fabrication.[1–3] For metal-oxide semiconductors, superior field-effect mobility (μ_{eff}) ranging from 20 to 100 cm^2/Vs is attractive for high-speed, high-resolution, and large-area display panels.[1–3] In particular, nano-crystalline IZO in the amorphous matrix has been considered as an alternative to the more commonly used wide-bandgap oxides.[4–6] Nano-crystalline phase can provide a negligible distribution of device characteristics.[6] So far, oxide thin-film transistors have primarily been studied for switching devices for display and semiconductor applications.[7–16] However, IZO–TFTs can also be used as photosensors, especially for visible photo-sensor applications.[17–25]

IZO is well known for its optical properties such as high photoconductivity and persistent photoconductivity (PPC).[17–25] Both properties in IZO photo-transistors were analyzed in this study, taking into account the sub-gap optical absorption due to oxygen vacancy.[17–25] Under illumination, the increase in photocurrent is relevant to the ionization energy of V_o to V_o^{++} (Refs. 17–25). This is accompanied by structural relaxation, which causes PPC. In TFT structured sensor, negative gate is typically used for read operation due to high photocurrent ratio.[17] Here, in the illumination, photo-induced V_o^{++} screens the negative gate bias, leading to the formation of a un-depleted conductive channel, which lies far from the front interface.[12–25] Back channels under illumination exhibit high photoconductivity and PPC.[6,13,17,20–25] The charged particles such as V_o^{++}s have an effect on the photo-electrical and optical properties of photo-transistor.[5,6] Also, in another report, high photoconductivity in metal-oxide semiconductor materials is attributed to the extended electron lifetime, which results from retarded recombination due to hole localization.[26,27] The gradual increase in the photoconductivity of the oxide photo-transistor can be explained by reducing the transit time associated with short channel lengths.[26,27] In our investigation, we studied the photoconductivity of IZO–TFTs with varying device geometry. In particular, the ratio of photocurrent to dark current defined as the photosensitivity increases anomalously with decreasing channel length. Here, we present the origin of an anomalous high photoconductivity phenomenon in short-channel devices.

In order to look into high photoconductivity in IZO–TFTs, we studied drain current versus time and capacitance voltage (CV) versus characteristics of devices with various channel lengths and widths before and after illumination. The devices with channel lengths (L) of 5, 10, 15, and 20 μm with a channel width (W) of 100 μm were exposed to white light. The change in photoconductivity measured at $V_{GS} = -5$ V and $V_{DS} = 1$ V under this illumination is shown in Fig. 1(a). For a short-channel device ($L = 5\ \mu$m), the conductivity of the device upon light exposure was increased by roughly two orders of magnitude from the dark conductivity. On the other hand, the decay transient characteristic depicts typical PPC phenomenon. However, for long channel device, this behavior is not valid. For long channel device ($L = 20\ \mu$m), there is negligible photosensitivity of device. The drain current versus time measurements before and after illumination present significant channel length dependency. Consequently, typical PPC phenomenon is not observed in IZO–TFTs with a channel length of 20 μm or greater. The

a)Author to whom correspondence should be addressed. Electronic mail: jeonsh@korea.ac.kr

 © 2015 AIP Publishing LLC

This article is copyrighted as indicated in the article. Reuse of AIP content is subject to the terms at: http://scitation.aip.org/termsconditions. Downloaded to IP: 35.8.11.3 On: Tue, 26 Jan 2016 18:52:14

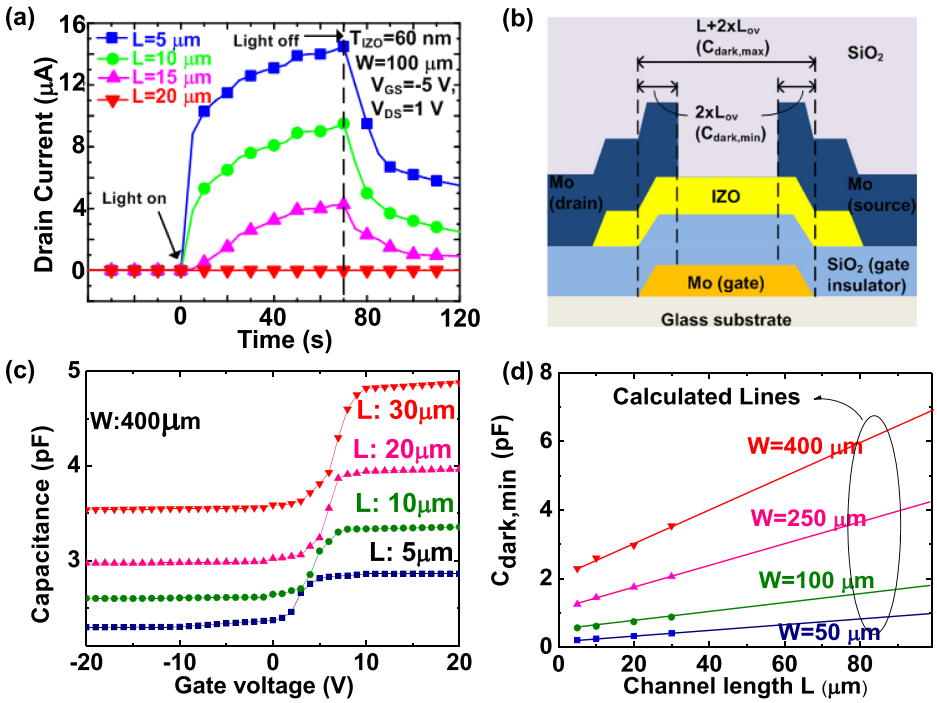

FIG. 1. (a) Time response for the photoconductivity measured under dark and illuminated conditions at $V_{GS} = -5$ V and $V_{DS} = 1$ V for IZO–TFTs with L of 5, 10, 15, and 20 μm at W of 100 μm, where IZO layer thickness is 60 nm. (b) Schematic diagram related to $C_{dark,min}$ and $C_{dark,max}$ including the layout components. (c) C_{dark} with various channel lengths (L = 5, 10, 20, and 30 μm) at W = 400 μm with an IZO layer thickness of 60 nm. $C_{dark,min}$ shows the channel-length dependency. The calculated $C_{dark,min}$ and $C_{dark,max}$ are also drawn by solid lines. (d) The measured $C_{dark,min}$ (symbols) and the theoretical $C_{dark,min}$ (lines) for various channel lengths and channel widths.

threshold of gate length is the function of IZO active semiconductor thickness and drain bias. For a relatively thick active semiconductor (>80 nm) and high V_{DS} (>20 V) condition, the threshold of gate length is shifted toward relative long channel toward 50 μm and beyond.

As an additional test, we performed CV measurements at $f = 1$ MHz with various channel lengths ($L = 5$, 10, 20, and 30 μm) and channel widths ($W = 100$, 250, and 400 μm) before and after illumination. In our CV measurement, there is negligible frequency dispersion in the measurement frequency. A 1 MHz test frequency is traditionally specified in C-V test procedures.[28] The three-terminal CV measurements were performed by connecting source and drain electrodes to a ground. In previous studies, the CV measurements under illumination were used for extracting the density of states of gallium-indium-zinc-oxide (GIZO) TFTs using the following functions:[29]

$$\frac{1}{C_{dark}(V_{GS})} = \frac{1}{C_{ox}} + \frac{1}{C_B(V_{GS})}, \tag{1}$$

$$\frac{1}{C_{photo}(V_{GS})} = \frac{1}{C_{ox}} + \frac{1}{C_B(V_{GS}) + C_{channel}}, \tag{2}$$

where C_{dark} is the measured capacitance in the dark, C_{photo} is the measured capacitance under illumination, C_{ox} is the gate oxide insulator capacitance, C_B is the capacitance due to the V_{GS}-responsive localized trapped charge, and $C_{channel}$ is the capacitance due to photo-responsive charges. C_{dark} as a function of the layout of the components can be as follows:[30]

$$C_{dark,\min} = \frac{C_{ox} \times C_{IZO}}{C_{ox} + C_{IZO}} \times 2 \times (L_{ov} + L_1) \times (W + 2 \times W_1), \tag{3}$$

$$C_{dark,\max} = C_{ox} \times (L + 2 \times (L_{ov} + L_0)) \times (W + 2 \times (W_{IZO} + W_0)), \tag{4}$$

where $C_{dark,min}$ is the measured minimum capacitance in dark, $C_{dark,max}$ is the measured maximum capacitance in dark, C_{IZO} is the channel capacitance, L_{ov} is the overlap length between gate and source/drain, and W_{IZO} is the width of the region between the gate and the IZO active layer (see Fig. 1(b)). The values of L_{ov} and W_{IZO} are 10 and 7 μm, respectively. $C_{dark,min}$ is mainly affected by L_{ov} and $C_{dark,max}$ is affected by the area of the entire channel region. Based on these values under dark conditions, we can extract model parameters. The extracted L_0 and W_0 are both 5 μm. The extracted L_1 and W_1 are both dependent on the geometry, in which L_1 is $0.29 \times L$ and W_1 is $0.2 \times W$. The geometric components in $C_{dark,min}$ with the channel-length (L_1) are easily determined by the results shown in Fig. 1(c) (W = 400 μm). The corresponding $C_{dark,min}$ and $C_{dark,max}$ are drawn as solid lines in Fig. 1(c), presenting a strong consistency with the experimental results. The theoretical $C_{dark,min}$ values for various channel lengths and widths are shown in Fig. 1(d) as solid lines, with symbols indicating the measured results.

C_{photo} was measured under illumination as well. For a simple comparison, we assume that the measured capacitances $C_{channel}$ are proportional to the active areas, $(L + 2 \times (L_{ov} + L_0)) \times (W + 2 \times (W_{IZO} + W_0))$. Using Eqs. (1) and (2), $C_{channel}$ was calculated. The measured C_{dark} and C_{photo} with various channel lengths and $W = 100$ μm are shown in Fig. 2(a) for comparison. At a glance, the C_{photo} of 5 μm-length device is greatly increased in the negative gate bias (off-current) region. The calculated $C_{channel}$ with various channel lengths and $W = 100$ μm is shown in Fig. 2(b), which can be converted to density of states ($g(E)$).[29] The extracted $g(E)$ values are roughly 4×10^{17} cm^{-3}eV^{-1} for L = 5 μm and $1.5–1.6 \times 10^{16}$ cm^{-3}eV^{-1} for $L = 10$, 20, and 30 μm, respectively. However, since all devices were prepared under the same experimental conditions, there is no clear explanation to account for a high $g(E)$ in short-channel IZO devices. Even if a small device is likely to be sensitive to edge

This article is copyrighted as indicated in the article. Reuse of AIP content is subject to the terms at: http://scitation.aip.org/termsconditions. Downloaded to IP: 35.8.11.3 On: Tue, 26 Jan 2016 18:52:14

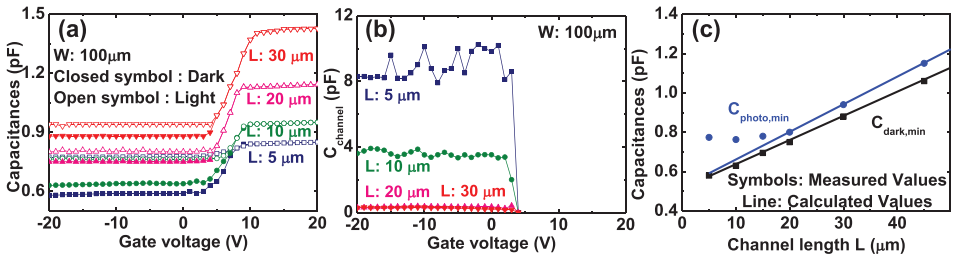

FIG. 2. (a) C_{dark} and C_{photo} with various channel lengths (L = 5, 10, 20, and 30 μm) at W = 100 μm with an IZO-layer thickness of 60 nm. (b) The calculated $C_{channel}$ with various channel lengths (L = 5, 10, 20, and 30 μm) at W = 100 μm. In short-channel devices, $C_{channel}$ is almost 10 times higher than that in long-channel devices. (c) The measured $C_{dark,min}$ and C_{photo} are shown as symbols with various channel lengths and W = 100 μm. The theoretical results with $g(E) = 1.5 \times 10^{16}\,cm^{-3}eV^{-1}$ are drawn as solid lines. The wide gap between the measured and the theoretical results is observed only in short-channel devices after illumination.

damage, its effect is probably negligible because we used the etch stopper structure.[31] The theoretical $C_{dark,min}$ and C_{photo} based on Eqs. (1)–(3) with geometric parameters and with $g(E) = 1.5 \times 10^{16}\,cm^{-3}eV^{-1}$ are shown in Fig. 2(c) as solid lines. The measured results for various channel lengths are shown as symbols in comparison. The considerable gap between measured and theoretical results is observed only in short-channel devices. This indicates that an additional factor aside from $g(E)$ is responsible for the change in C_{photo}.

For clear explanation of the channel length dependent $C_{dark,min}$ and C_{photo} values, we compared three-terminal CV measurement results (source/drain terminals are connected to ground) with two-terminal CV results (either source/drain is opened and the other contact is grounded). By using this method, the geometric components for the overlap region between gate and source/drain can be compared. Fig. 3(a) shows two and three-terminal CV measurement results for the device with $L = 5$ μm and $W = 200$ μm. In the same manner, Figs. 3(b) and 3(c) show the results for devices with $L = 10$ and 20 μm, respectively. In the long-channel device ($L = 20$ μm), the two-terminal CV measurement shows only a minor difference before and after illumination. If there is any edge damage during the fabrication process leading to high $g(E)$ in the short-channel devices, one should notice a similar disparity in these two-terminal measurements under illumination in the long-channel devices. However, negligible difference in C_{min_dark} and C_{photo} of long-channel device before and after illumination support the fact that edge damage does not increase the related $g(E)$. Therefore, a new hypothesis should be considered to explain the observed CV results, excluding the high $g(E)$ in the short-channel devices reflected from the edge damage.

In the dark condition, when we compare with two and three-terminal CV measurement results, $C_{min,dark}$ is only dependent on L_{ov} and thus the $C_{min,dark}$ by the two-terminal method is half of that measured by the three-terminal method for all channel lengths. According to this relation, we plotted additional red dotted lines that correspond to half of the C_{min} measured by the three-terminal CV method for devices with $L = 5$, 10, and 20 μm before and after illumination, as seen in Figs. 3(a)–3(c). The measured $C_{min,dark}$ values from the two-terminal method should be exactly half of those from the three-terminal method for all channel lengths. However, after illumination, this circumstance is not maintained. For a short channel device ($L = 5$ μm), the C_{min} value obtained by the two-terminal CV measurement is greater than half of the

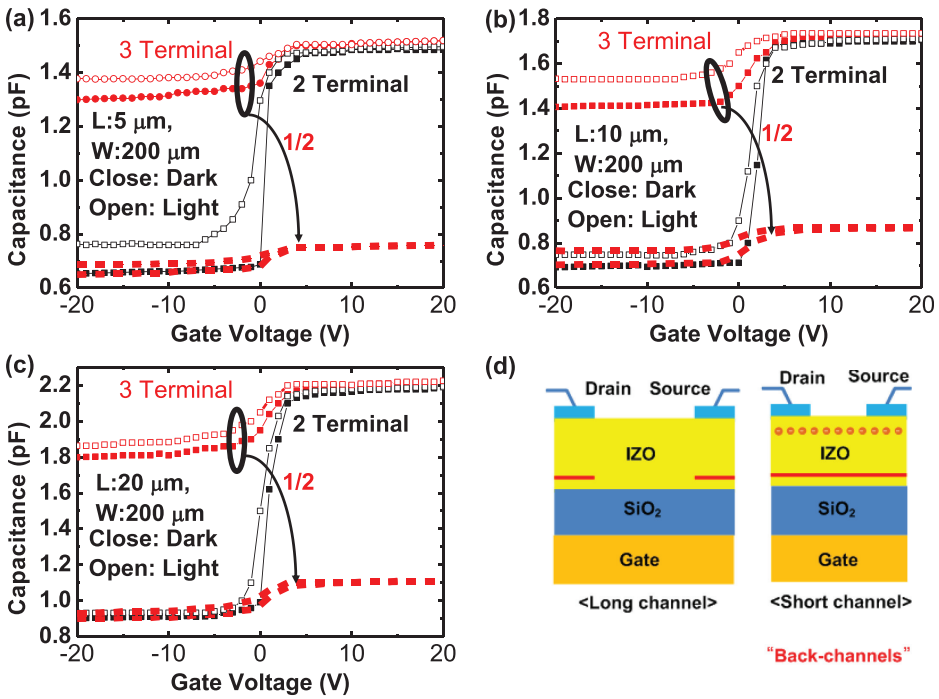

FIG. 3. Two-terminal and three-terminal CV measurement results of devices with (a) L = 5 μm, (b) L = 10 μm, and (c) L = 20 μm with W = 200 μm, in dark and under the light illumination. (d) Schematic diagram related to the proposed model. The equipotential region is generated by the field between the gate and the drain/source only in short-channel devices. This equipotential region gathers charge carriers, and it can be referred to as a "back-channel."

This article is copyrighted as indicated in the article. Reuse of AIP content is subject to the terms at: http://scitation.aip.org/termsconditions. Downloaded to IP: 35.8.11.3 On: Tue, 26 Jan 2016 18:52:14

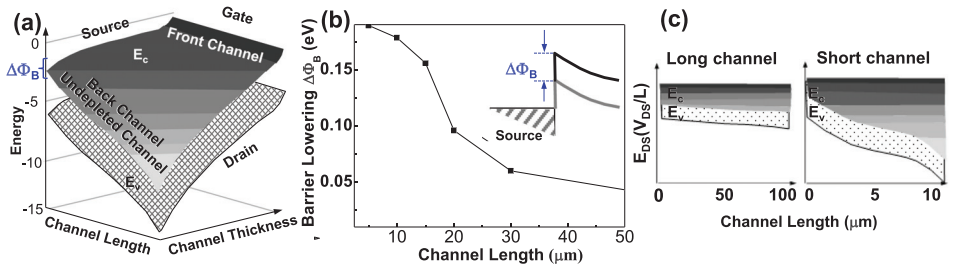

FIG. 4. (a) 3D device structure at V_{GS} of −7V and V_{DS} of 10 V under the illumination state (b) the reduced barrier height of source to gate barrier with respect to gate length. (c) 3D band diagram along the channel from source to drain with long (left) and short (right) channel devices. For short channel device, the back channel is not depleted even under negative gate bias condition, forming equipotential conducting channel from source to drain.

C_{min} value observed by the three-terminal CV method (Fig. 3(a)), while long channel devices (Figs. 3(b) and 3(c)), the C_{min} value obtained by the two-terminal CV measurement is half of the C_{min} value observed by the three-terminal CV method. It suggests that in the two-terminal CV method, a conducting equipotential region is existed nearby the grounded source/drain electrode only in short-channel devices under illumination. It is possible that this equipotential region is generated by the field between the gate and the drain/source. Also, for a short channel device under illumination, the C_{min} value is almost comparable to C_{max} (0.92 C_{min}). So we can speculate that a significant part of conducting region is existed along with channel for a short channel device. Considering that negative gate bias is applied for achieving high photosensitivity and photo-induced V_o^{++}s screen negative gate bias, it suggests that the un-depleted back channel is formed, thereby generating conducting channel. This region plays an important role in carrier transport and can be referred to as "back-channels." A schematic diagram is presented in Fig. 3(d).

In order to further verify the existence of back channel for a short channel device under the illumination, we performed three-dimensional device simulation and extracted the barrier lowering ($\Delta\phi_b$) from the photocurrent data Figures 4(a) and 4(b). In order to simulate the effect of V_o^{++} under the light state at a given bias condition, we put the positive fixed charges in the front channel and posed V_{GS} of −7 V and V_{DS} of 10 V. Since we apply negative gate bias, the band of the front channel is bent upward. Due to the effect of positive charges in semiconductor, we observe source side barrier lowering. From the photocurrent data with channel length, the barrier lowering height was extracted and that of short channel device is significant (Fig. 4(b)), leading to anomalous high photocurrent of short channel device. As we take a look at the E_c and E_v of back channel along the channel length for short and long channel devices (see Fig. 4(c)), both E_c and E_v for short channel device is bent downward due to a combined effect of relatively high lateral field and the existence of V_o^{++}, forming the conducting back channel from source to drain.

We examined channel length dependent photoconductivity using current to time, DC, and CV measurements. In IZO TFTs, high photo-conductivity and PPC are only observable in short channel devices. This channel length dependent photocurrent and PPC phenomenon are relevant to un-depleted back channel. This region plays an important role in carrier transport at "back-channels" by the field between the gate and the source/drain only in short-channel devices under the illumination.

This work was supported by the National Research Foundation of Korea (NRF) grant funded by the Korean Government (MEST) (No. 2014R1A2A2A01006541).

[1]P. Barquinha, G. Goncalves, L. Pereira, R. Martins, and E. Fortunato, Thin Solid Films **515**, 8450 (2007).
[2]D. Paine, B. Yaglioglu, Z. Beiley, and S. Lee, Thin Solid Films **516**, 5894 (2008).
[3]R. Martins, P. Almeida, P. Barquinha, L. Pereira, A. Pimentel, I. Ferreira, and E. Fotunato, J. Non-Cryst. Solids **352**, 1471 (2006).
[4]T. Kamiya and H. Hosono, NPG Asia Mater. **2**, 15 (2010).
[5]E. Fortunato, P. Barquinha, and R. Martins, Adv. Mater. **24**(22), 2945 (2012); E. Fortnato, P. Barquinha, A. Pimentel, A. Goncalves, A. Marques, R. Martins, and L. Pereira, Appl. Phys. Lett. **85**, 2541 (2004).
[6]D.-H. Cho, S. Yang, S.-H. K. Park, C. Byun, S.-M. Yoon, J.-I. Lee, C.-S. Hwang, H. Y. Chu, and K. Cho, SID Symp. Dig. Tech. Pap. **40**, 280 (2009); H. Oh, S.-M. Yoon, M. Ryu, C.-S. Hwang, S. Yang, and S. Park, Appl. Phys. Lett. **97**, 183502 (2010).
[7]H.-S. Choi and S. Jeon, Appl. Phys. Lett. **104**, 023505 (2014).
[8]H. Kim, S. Jeon, M.-J. Lee, J. Park, S. Kang, H.-S. Choi, C. Park, H.-S. Hwang, C. Kim, J. Shin *et al.*, IEEE Trans. Electron Devices **58**(11), 3820 (2011).
[9]T.-Y. Hsieh, T.-C. Chang, T.-C. Chen, Y.-C. Chen, and Y.-T. Chen, Appl. Phys. Lett. **101**, 212104 (2012).
[10]P. Barquinha, A. Pimentel, A. Marques, L. Pereira, R. Martins, and E. Fourtnato, J. Non-Cryst. Solids **352**, 1749 (2006).
[11]S. Kim, S. Kim, C. Kim, J. Park, I. Song, S. Jeon, S. Ahn, J. Park, and J. Jeong, Solid State Electron. **62**, 77–81 (2011).
[12]S. Jeon, S. Park, I. Song, J.-H. Hur, J. Park, H. Kim, S. Kim, S. Kim, H. Yin, U.-I. Chung *et al.*, ACS Appl. Mater. Interfaces **3**, 1 (2011).
[13]H.-S. Choi, S. Jeon, H. Kim, J. Shin, C. Kim, and U.-I. Chung, Appl. Phys. Lett. **100**, 173501 (2012).
[14]S. Jeon, S. Park, I. Song, J.-H. Hur, S. Kim, S. Kim, H. Yin, E. Lee, S. Ahn, H. Kim *et al.*, IEEE Int. Electron Devices Meet. **2010**, 21.3.1–21.3.4.
[15]S. Jeon, A. Benayad, S. Ahn, S. Park, I. Song, C. Kim, and U.-I. Chung, Appl. Phys. Lett. **99**, 082104 (2011).
[16]S. Jeon, H. Kim, H. Choi, I. Song, S. Ahn, C. Kim, J. Shin, U. Chung, I. Yoo, and K. Kim, Symp. VLSI Technol., Dig. Tech. Pap. **2011**, 978.
[17]S. Park, S. Park, S. Ahn, I. Song, W. Chae, M. Han, J. Lee, and S. Jeon, J. Vac. Sci. Technol., B **31**, 050605 (2013).
[18]P.-T. Liu, Y.-T. Chou, and L.-F. Teng, Appl. Phys. Lett. **94**, 242101 (2009).
[19]S. Jeon, S. Kim, S. Park, I. Song, J. Park, S. Kim, and C. Kim, IEEE Electron Device Lett. **31**(10), 1128 (2010).
[20]S. Jeon, S.-E. Ahn, I. Song, C. J. Kim, U.-I. Chung, E. Lee, I. Yoo, A. Nathan, S. Lee, J. Robertson, *et al.*, Nat. Mater. **11**, 301 (2012).
[21]S.-E. Ahn, I. Song, S. Jeon, Y. Jeon, Y. Kim, C. Kim, B. Ryu, J. Lee, A. Nathan, S. Lee *et al.*, Adv. Mater. **24**, 2631–2636 (2012).
[22]S. Jeon, I. Song, S. Lee, B. Ryu, S. Ahn, E. Lee, Y. Kim, A. Nathan, J. Robertson, and U.-I. Chung, Adv. Mater. **26**, 7102 (2014).
[23]S. Lee, S. Ahn, Y. Jeon, J. Ahn, I. Song, S. Jeon, D. Yun, J. Kim, H. Choi, U.-I. Chung *et al.*, Appl. Phys. Lett. **103**, 251111 (2013).

This article is copyrighted as indicated in the article. Reuse of AIP content is subject to the terms at: http://scitation.aip.org/termsconditions. Downloaded to IP: 35.8.11.3 On: Tue, 26 Jan 2016 18:52:14

[24]S.-E. Ahn, S. Jeon, Y. Jeon, C. Kim, J. Lee, C. Lee, J. Park, I. Song, A. Nathan, S. Lee *et al*., Adv. Mater. **25**, 5549–5554 (2013).
[25]H. Choi and S. Jeon, Appl. Phys. Lett. **104**, 133507 (2014).
[26]A. Nathan, S. Lee, S. Jeon, and J. Robertson, J. Disp. Technol. **10**(11), 917 (2014).
[27]S. Lee, S. Jeon, J. Robertson, and A. Nathan, IEEE Int. Electron Devices Meet. **2012**, 542.
[28]S. Jeon and S. Park, Microelectron. Eng. **88**, 872–876 (2011).
[29]K. Jeon, C. Kim, I. Song, J. Park, S. Kim, S. Kim, Y. Park, J.-H. Park, S. Lee, D. M. Kim *et al*., Appl. Phys. Lett. **93**, 182102 (2008).
[30]S. Lee, Y. W. Jeon, S. Kim, D. Kong, D. H. Kim, and D. M. Kim, Solid State Electron. **56**, 95 (2011).
[31]M. Kim, J. Jeon, H. Lee, T. Ahn, H. Shin, J. Park, J. Jeong, Y. Mo, and H. Kim, Appl. Phys. Lett. **90**, 212114 (2007).

This article is copyrighted as indicated in the article. Reuse of AIP content is subject to the terms at: http://scitation.aip.org/termsconditions. Downloaded to IP: 35.8.11.3 On: Tue, 26 Jan 2016 18:52:14